The Astrophysical Journal, 721:1579–1584, 2010 October 1 doi:10.1088/0004-637X/721/2/1579

EVIDENCE FOR INTERNAL TETHER-CUTTING IN A FLARE/CORONAL MASS EJECTION OBSERVED BY *MESSENGER*, *RHESSI*, AND *STEREO*

Claire L. Raftery[1], Peter T. Gallagher, R. T. James McAteer, Chia-Hsien Lin[2], and Gareth Delahunt
Astrophysics Research Group, School of Physics, Trinity College Dublin, Dublin 2, Ireland; claire@ssl.berkeley.edu
Received 2009 October 2; accepted 2010 July 27; published 2010 September 10

ABSTRACT

The relationship between eruptive flares and coronal mass ejections (CMEs) is a topic of ongoing debate, especially regarding the possibility of a common initiation mechanism. We studied the kinematic and hydrodynamic properties of a well-observed event that occurred on 2007 December 31 using data from *MESSENGER*, *RHESSI,* and *STEREO* in order to gain new physical insight into the evolution of the flare and CME. The initiation mechanism was determined by comparing observations to the internal tether-cutting, breakout, and ideal magnetohydrodynamic (MHD) models. Evidence of pre-eruption reconnection immediately eliminated the ideal MHD model. The timing and location of the soft and hard X-ray sources led to the conclusion that the event was initiated by the internal tether-cutting mechanism. In addition, a thermal source was observed to move in a downward direction during the impulsive phase of the event, followed by upward motion during the decay phase, providing evidence for X- to Y-type magnetic reconnection.

Key words: Sun: coronal mass ejections (CMEs) – Sun: flares

Online-only material: color figures

1. INTRODUCTION

Gosling (1993) postulated that geomagnetic storms are produced by coronal mass ejections (CMEs) and not, as previously thought, by solar flares. This declaration, dubbed "the solar flare myth," led to the misunderstanding that solar flares were not an important aspect of solar physics research as they had no effect on life on Earth. This belief divided the community and was contested on numerous occasions (e.g., Hudson et al. 1995; Reames 1995; Švestka 2001). The significance of solar flares has since been restored and was summarized nicely by Švestka (2001): "It is misleading to claim that flares are not important in solar–terrestrial relations. Although they do not cause the CME phenomenon that propagates from the Sun eventually hitting the Earth, they are excellent indicators of coronal storms and actually indicate the strongest, fastest, and the most important storms." Since then, the ideas connecting flares and CMEs have moved away from the cause and effect paradigm, and it is now widely accepted that eruptive flares and CMEs both result from the same driving mechanism (Zhang et al. 2001).

The behavior of CMEs and eruptive flares have been investigated on two fronts—theoretically and observationally. Unfortunately, the comparison between theory and observations is difficult and in most cases is a qualitative one. The mechanism involved in the initiation of CMEs is still a topic of hot debate with many competing theories. The three models summarized in Moore & Sterling (2006) are used for a qualitative comparison to observations in this paper. These are the internal tether-cutting, external tether-cutting, and ideal magnetohydrodynamic (MHD) instability mechanisms for driving CME eruptions.

The internal tether-cutting picture begins with a sheared central core tethered by a central arcade (Moore & Roumeliotis 1992; Moore & Sterling 2006). Neighboring arcades may also be present but are not explicitly required. Before eruption, the central arcade is in force-free equilibrium and no current sheet exists between it and the overlying field. However, a current sheet does exist between the legs of the arcade as a result of their slow shearing due to photospheric motions. When this current sheet becomes sufficiently thin to allow reconnection across it, a runaway tether-cutting process begins. The field lines above the reconnection site (the plasmoid) are no longer tethered to the photosphere and begin to erupt upward while the field lines beneath the reconnection site reconnect to become a solar flare. In the case of quadrupolar topology, the plasmoid erupts upward, forming a current sheet between it and the overlying field. This results in explosive breakout reconnection above the plasmoid, leading to restructuring of the neighboring/overlying field as they reconnect, both heating the side arcades and removing the overlying field blocking the path of the plasmoid.

The external tether-cutting, or breakout, model begins with a quadrupolar magnetic topology (Antiochos 1998; Antiochos et al. 1999). The structure inside the central arcade is such that magnetic reconnection is not allowed between the arcade legs but can occur between the top of the arcade and the overlying field. This can result from further emergence of the central arcade, which works to compress the current sheet between the central arcade and the overlying field without the generation of a current sheet between the arcade legs. Reconnection above the arcade can result in non-equilibrium conditions, forcing the central arcade to rise. This results in the stretching of the field lines, drawing the legs of the central arcade together to create a second current sheet between the footpoints along which reconnection can occur. This results in runaway tether-cutting reconnection as in the internal tether-cutting case. Unlike the internal tether-cutting case, however, breakout reconnection is the initiation mechanism responsible for the CME eruption, with internal reconnection occurring as a secondary effect. Therefore, evidence of heating or reconnection in the neighboring arcades would be expected before evidence of the same in the central arcade.

The third case we consider is the ideal MHD or catastrophe model (e.g., Forbes & Isenberg 1991; Forbes & Priest 1995; Isenberg et al. 1993). Unlike the first two models, this scenario

[1] Current address: Space Science Lab, UC Berkeley, 7 Gauss Way, Berkeley, CA 94720-7450, USA.
[2] Current address: Plasma and Space Science Center, National Cheng-Kung University, Taiwan.

is not triggered by magnetic reconnection. Instead, the continued shearing and twisting of the central arcade gradually evolves the field until it is forced out of force-free magnetostatic equilibrium. The field seeks a new equilibrium by erupting upward, generating two current sheets: one between the stretched fields of the arcade legs and the other between the top of the arcade and the overlying field. It has been shown that this can occur without the use of magnetic reconnection (e.g., Isenberg et al. 1993; Chen & Shibata 2000; Roussev et al. 2003). Following the formation of the current sheets, magnetic reconnection can take place and runaway tether-cutting drives the launch of the CME as before. Observational evidence for an ideal MHD trigger would involve the rising of the flux rope *before* any indication that magnetic reconnection had taken place.

Observationally, complete analyses of flare–CME systems have been hindered by the lack of suitable data. Considering the broad range of temperatures (∼8000 K to ∼20 MK), energies (few eV to MeV), and distances (1 to $>30\,R_{\odot}$), it is clear that a multi-instrument approach is necessary. In the past, the kinematics of CMEs (e.g., velocity, acceleration) have been well studied. Gallagher et al. (2002) presented the first observations of a rising soft X-ray (SXR) source that occurred in conjunction with a CME. The kinematics of the SXR loops were analyzed in detail and the thermal emission was found to originate from successively higher altitudes as the flare progressed, agreeing with the standard flaring picture. The acceleration of the associated CME was then investigated by Gallagher et al. (2003). Although the entire flare/CME system was analyzed by Gallagher et al. (2002, 2003), the critical connection between the flare and CME was not specifically investigated until Temmer et al. (2008) found that the CME acceleration occurs simultaneously with the hard X-ray (HXR) burst of the corresponding flares. This lends further support to the conclusions of Zhang et al. (2001), who suggested that CMEs and flares are driven by the same mechanism but do not have a cause and effect relationship. The importance of the flare–CME onset has been well documented by Harrison & Bewsher (2007). Using the evolution of the pre-flare arcades through a series of extreme ultraviolet (EUV) spectroscopic observations, they established the importance of the pre-eruption activity. Often, the temperature and density (emission measure) evolution of a system is conducted using spectroscopic data, such as that used in Harrison & Bewsher (2007) and Raftery et al. (2009). However, since these instruments are most effective close to disk center, observations of limb flares are not as readily available. An alternative method of studying flare hydrodynamics is to use the spectroscopic capabilities of the *Reuven Ramaty High Energy Solar Spectroscopic Imager* (*RHESSI*; Lin et al. 2002). However, since *RHESSI* is primarily designed to study high-energy emission, caution must be taken when analyzing the lower energy end of the spectrum ($\lesssim$6 keV), especially when the attenuators are in use. As such, while high-temperature emission can be modeled accurately with *RHESSI*, lower temperature emission ($\lesssim$5 MK while in the A1 state) is harder to observe. By comparison, the kinematics of CMEs originating on the limb are better observed than those originating on disk. For limb events, the components of the CME can be easily observed against the sky and avoid contamination by disk emissions. As a result of these obstacles, the hydrodynamic evolution of eruptive flares with well-observed CMEs are rare.

In this paper, the hydrodynamic evolution of a CME-associated solar flare is examined in a unique way, using the Solar Array for X-rays (SAX; Schlemm et al. 2007) on board the *Mercury Surface, Space Environment, Geochemistry and Ranging* (*MESSENGER*; Santo et al. 2001). The temperature and emission measure of the flare is investigated in conjunction with the kinematic evolution of both the CME and the post-flare loop system. The availability of this unique data set has facilitated this extensive study. The instruments used were located throughout the heliosphere and provided excellent coverage of the event, both temporally and spectrally. Along with *MESSENGER*/SAX, the instruments used included *GOES-12*, *RHESSI*, and the Extreme Ultraviolet Imager (EUVI), Cor 1, and Cor 2 instruments in the Sun Earth Connection Coronal and Heliospheric Investigation suite (SECCHI; Howard et al. 2008) on board the Behind spacecraft of the *Solar Terrestrial Relations Observatory* (*STEREO*; Kaiser et al. 2008). The observations and data analysis techniques are discussed in Section 2. Section 3 describes the main results of this investigation which are discussed in light of current theory in Section 4.

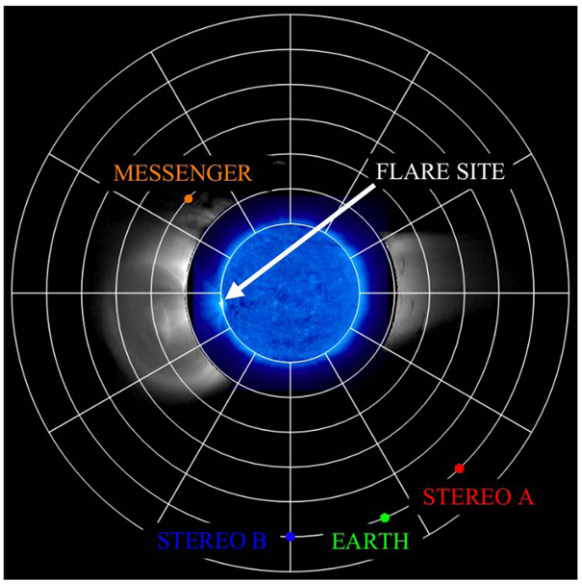

Figure 1. Position of the spacecraft used to observe the flare–CME event on 2007 December 31. *RHESSI* and *GOES* are orbiting Earth. This is a top-down grid overlaid on a side-on image taken with 171 Å *STEREO B*/EUVI (blue) and Cor 1 (black and white).

(A color version of this figure is available in the online journal.)

2. OBSERVATIONS AND DATA ANALYSIS

The event under consideration occurred on the east limb of the Sun on 2007 December 31. The SXR flux began to rise from approximately 00:30 UT. The CME was launched at 00:48 UT and the SXR flux was above background levels for more than 4 hr. As observed from Earth, the footpoints in the low corona were occulted. Therefore, Earth orbiting satellites (*RHESSI* and *GOES*) observed only loop-top emission from the event. As a result, it is likely that the *GOES* classification of C8.3 is an underestimation of the total flux. *STEREO B* and *MESSENGER*, however, both had unobstructed views of the entire system, as Figure 1 shows.

2.1. X-ray Spectroscopy

The *RHESSI* A1 attenuators were in place for the duration of this event. As such, the *RHESSI* spectrum was only analyzed above 6 keV. The thermal continuum was well modeled using an isothermal distribution and the non-thermal emission was

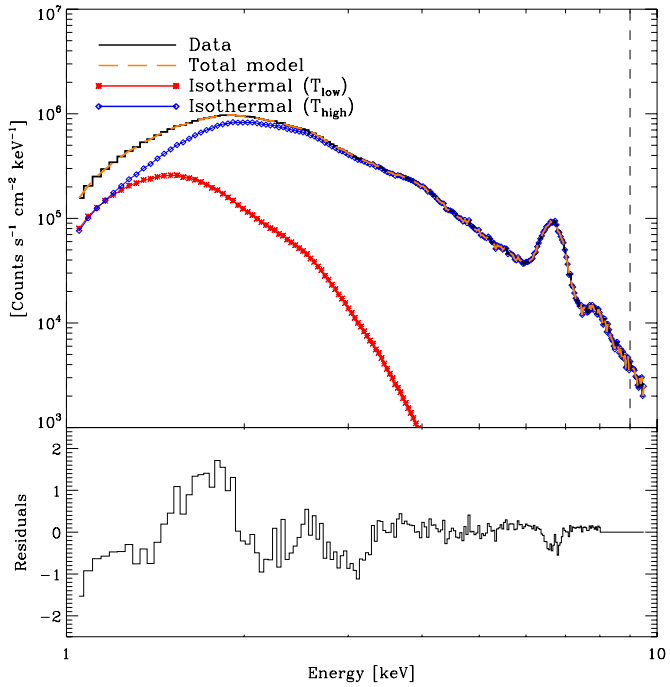

Figure 2. Top panel shows the *MESSENGER*/SAX spectrum from the peak of the flare between 00:47 UT and 00:52 UT (solid black line). The isothermal fits are shown as red asterisks (low temperature) and blue diamonds (high temperature). The normalized residuals are shown in the bottom panel.

(A color version of this figure is available in the online journal.)

modeled using a broken power law. The temperature and emission measure were calculated during the early decay phase of the event by fitting the thermal part of the *RHESSI* spectrum with a Maxwell distribution. As the lower energy range of the spectrum (<6 keV) was not analyzed due to the attenuator state, any plasma with a temperature of $\lesssim$5 MK present in the loop was not observed with *RHESSI*. The *MESSENGER*/SAX instrument was used to account for any low-temperature emission. This instrument is designed to measure characteristic X-ray emissions from the surface of Mercury. Incident solar flux is measured using SAX for calibration purposes (when analyzing Mercury). SAX, a Silicon-PIN detector mounted on the spacecraft sunshade (Schlemm et al. 2007), is sensitive in the 1–10 keV range, overlapping with the thermal range of the *RHESSI* spectrum. The SAX spectral resolution of 0.6 keV (Schlemm et al. 2007) is almost twice that of *RHESSI* (1 keV; Lin et al. 2002), which, along with SAX's sensitivity to lower energies, allows both high- and low-temperature emission to be observed and modeled accurately. Figure 2 shows a sample SAX spectrum taken at the peak of the flare. The spectra were fit using the SolarSoft SPEX package (Schwartz et al. 2002). Two isothermal functions were used to approximate a differential emission measure function to accommodate both high- and low-temperature plasma present in the flare.

2.2. Imaging

RHESSI images were reconstructed using the CLEAN algorithm and detectors 3, 4, 5, and 6 integrated over 2 minute periods. The source was imaged in the 3–6, 6–12, and 12–25 keV energy bands. The 30–50 keV coronal sources imaged by Krucker et al. (2010) have also been incorporated into this study. The evolution of the flare and the acceleration phase of the CME were imaged using the 171 Å filter of the EUVI instrument on

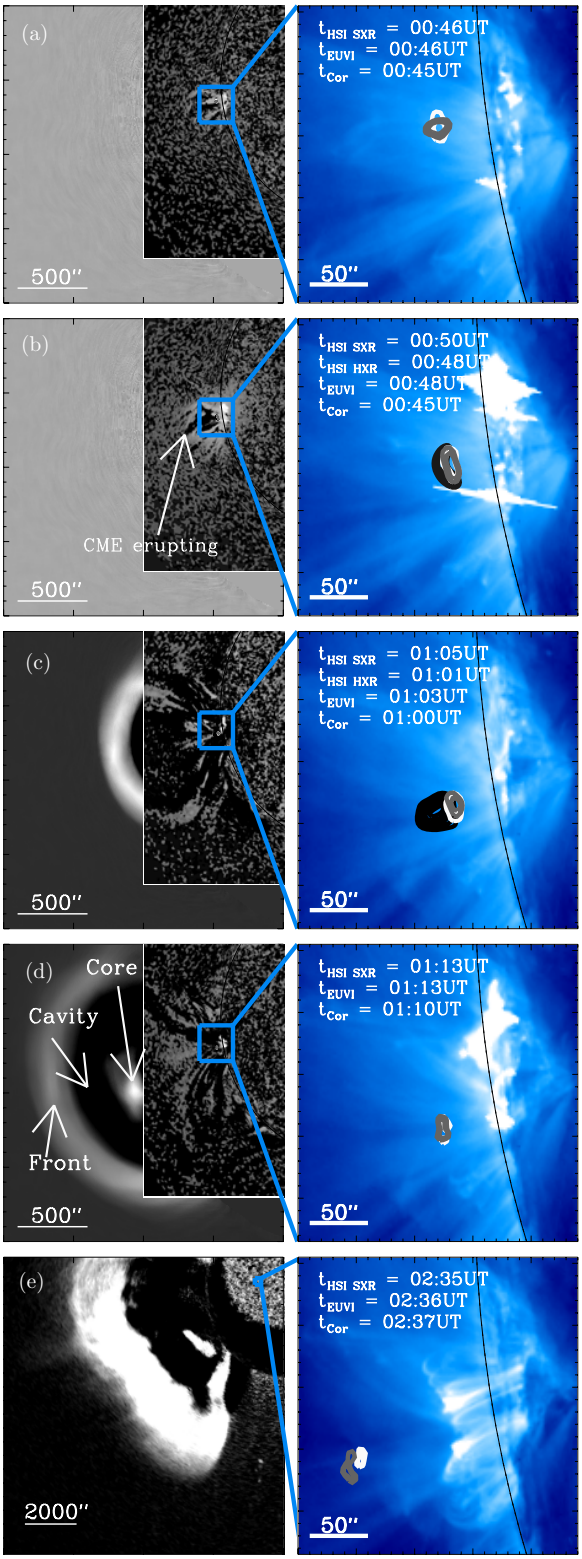

Figure 3. Evolution of the 2007 December 31 flare-CME as observed by EUVI 171 Å, Cor 1, Cor 2 (panel (e) only), *RHESSI* 3–6 keV (white), 6–12 keV (gray), and 30–50 keV (black).

(A color version of this figure is available in the online journal.)

board *STEREO B*, while the propagation phase of the CME was imaged using Cor 1 and Cor 2.

Figure 3 shows the evolution of the event. The left-hand panels are interlaced difference images from EUVI and Cor 1 and Cor 2

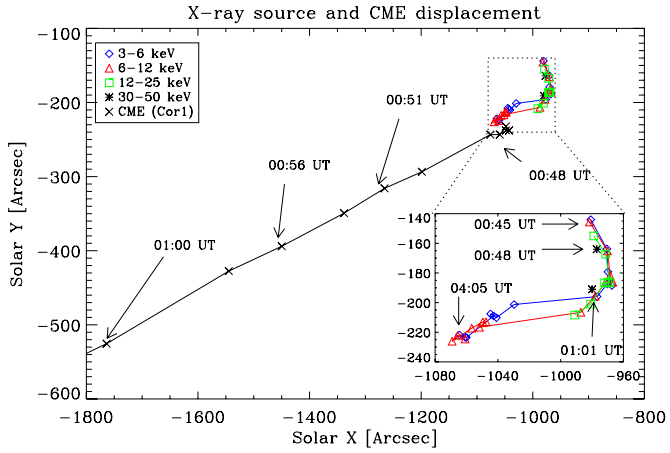

Figure 4. Position of the CME front in the Cor 1 field of view (black crosses) along with the centroid of the *RHESSI* sources: 3–6 (blue diamonds), 6–12 (red triangles), 12–25 (green squares), and 30–50 keV (black asterisks). The inset panel is a magnified view of the flaring region. Time stamps for both the flare and CME are also marked.

(A color version of this figure is available in the online journal.)

(panel (e) only). Overlaid on these are the *RHESSI* sources, 3–6 keV (white), 6–12 keV (gray), and 30–50 keV (black, panels (b) and (c) only). The flaring region of the event has been expanded on the right-hand side to highlight the evolution of a post-flare loop system and the motion of the SXR sources.

3. RESULTS

This CME–flare system was observed over more than 4 hr using a multitude of instruments. Figure 3 shows the evolution of the system and Figure 4 explicitly shows the motion of both the CME and SXR loop-top sources (inset). As *RHESSI* emerged from eclipse at ∼00:46 UT, an SXR source was observed to lie above and between two bright EUV ribbons (Figure 3(a)). Between 00:46 UT and 00:48 UT, the SXR sources appeared to move in a southerly direction, decreasing in altitude at the same time (Figure 4, inset). The decreasing altitude of the SXR source may correspond to the change from X- to Y-type reconnection (Sui & Holman 2003). At 00:48 UT (Figure 3(b)), a 30–50 keV coronal source was observed above the now extended thermal sources. Simultaneously, the CME was launched. Figure 3(b) also shows the location of the SXR source to be at the base of the CME, between the flare footpoints. Following the CME eruption, the SXR source began to rise beneath the CME while still moving along what would become the post-flare arcade. Figure 4 shows that the direction of motion of the post-flare loops follow the same path as the CME. Figure 3(c) shows a straight structure connecting the X-ray sources to the core of the CME, while in Figure 3(d) the three-part structure of the CME is clearly identifiable. The evolving post-flare arcade is also visible in this figure. The bottom panel of Figure 3 shows the system approximately 2 hr after eruption. The CME is observed in the Cor 2 field of view, the post-flare loop system has evolved and the X-ray sources are still located above the post-flare EUV loops, at the base of the CME.

Figure 5 shows the kinematics of the flare and the CME, along with the hydrodynamic evolution of the flare. The CME liftoff time (00:48 UT; defined as the time the CME is first observed by EUVI, marked in Figure 3(b)) is highlighted in each panel with a dashed vertical line. Figure 5(a) shows the displacement of the *RHESSI* SXR sources (3–6, 6–12, and 12–25 keV) relative to Sun center. The 30–50 keV sources are also shown here. The average velocity of the loops as they descend (pre 00:50 UT) is 18 ± 4 km s^{-1}. The height of the ascending loops (post 00:50 UT) were fit with a constant acceleration model:

$$h(t) = h_0 + v_0 t + \frac{1}{2} a t^2, \quad (1)$$

where h_0, v_0, and a, averaged across the three energy ranges, are 711.1 ± 0.5 Mm, 15 ± 2 km s^{-1}, and $-1.1 \pm 0.9 \times 10^{-3}$ km s^{-2}. These fits are shown in Figure 5(a).

Figure 5(b) shows the displacement of the CME apex relative to Sun center measured using the *STEREO B* instruments: EUVI, Cor 1, and Cor 2 (for a detailed study of the CME velocity and acceleration and a quantitative comparison to theoretical models, see Lin et al. 2010). Panel (c) of Figure 5 shows the *RHESSI* 25–50 keV HXR light curve (green). The peak in the HXRs corresponds exactly to the time the CME is launched. Overplotted on this is the *GOES* 1–8 Å light curve. It should be noted that the appearance of multiple peaks in the *GOES* light curve is as a result of occultation and not multiple events. This was verified by comparing EUV Imaging Telescope intensity (partially occulted) to that of EUVI on *STEREO B* (not occulted). Figure 5(d) shows the thermal evolution of the flare using results from *RHESSI*, SAX, and *GOES*. The *GOES* temperature (and later, emission measure) were obtained from the ratio of the two flux channels following Thomas et al. (1985). It is clear that the lower-temperature component of the SAX spectrum remains approximately constant during the initial and early decay phases of the flare while the higher-temperature component rises quickly to a maximum value of 19 ± 2 MK. The high- and low-temperature components converge as the flare decays. Figure 5(e) shows the evolution of emission measure of the flare, again from *RHESSI*, SAX, and *GOES*. As expected, the level of high-temperature emission increases as the flare approaches its peak. Surprisingly, however, the level of cooler emission also increases during the flare impulsive phase.

4. CONCLUSIONS AND DISCUSSION

This paper presents observations of a CME and associated solar flare that were studied using a range of spacecraft positioned at various positions in the heliosphere. The eruption took place on the east limb of the Sun and the footpoints were occulted as viewed from Earth. Before the eruption, an SXR source was observed in conjunction with increasing flare temperature and emission measure. At 00:48 UT, the time the CME was launched, a 30–50 keV HXR loop-top source was observed. Following the liftoff of the CME, the SXR source was found to rise beneath it as the temperature and emission measure both began to return to pre-eruption values. The SXR source became extended across the top of the arcade as the event progressed. This may be as a result of *RHESSI* observing the combined flux from many reconnecting loops as successive reconnection events progressing along the arcade in a similar fashion to the asymmetric eruption described in Tripathi et al. (2006).

The pre-eruption increase in temperature and emission measure, along with the presence of the SXR source early in the event is strong evidence for pre-eruption reconnection. Following the interpretation of Sui & Holman (2003), this event exhibits signs of X- to Y-type reconnection. Sui & Holman (2003) observed a loop-top source that appeared to shrink during the impulsive phase of a flare and rise during the decay phase. This apparent loop shrinkage is understood to result from changing the magnetic field configuration from an X-point to a current sheet.

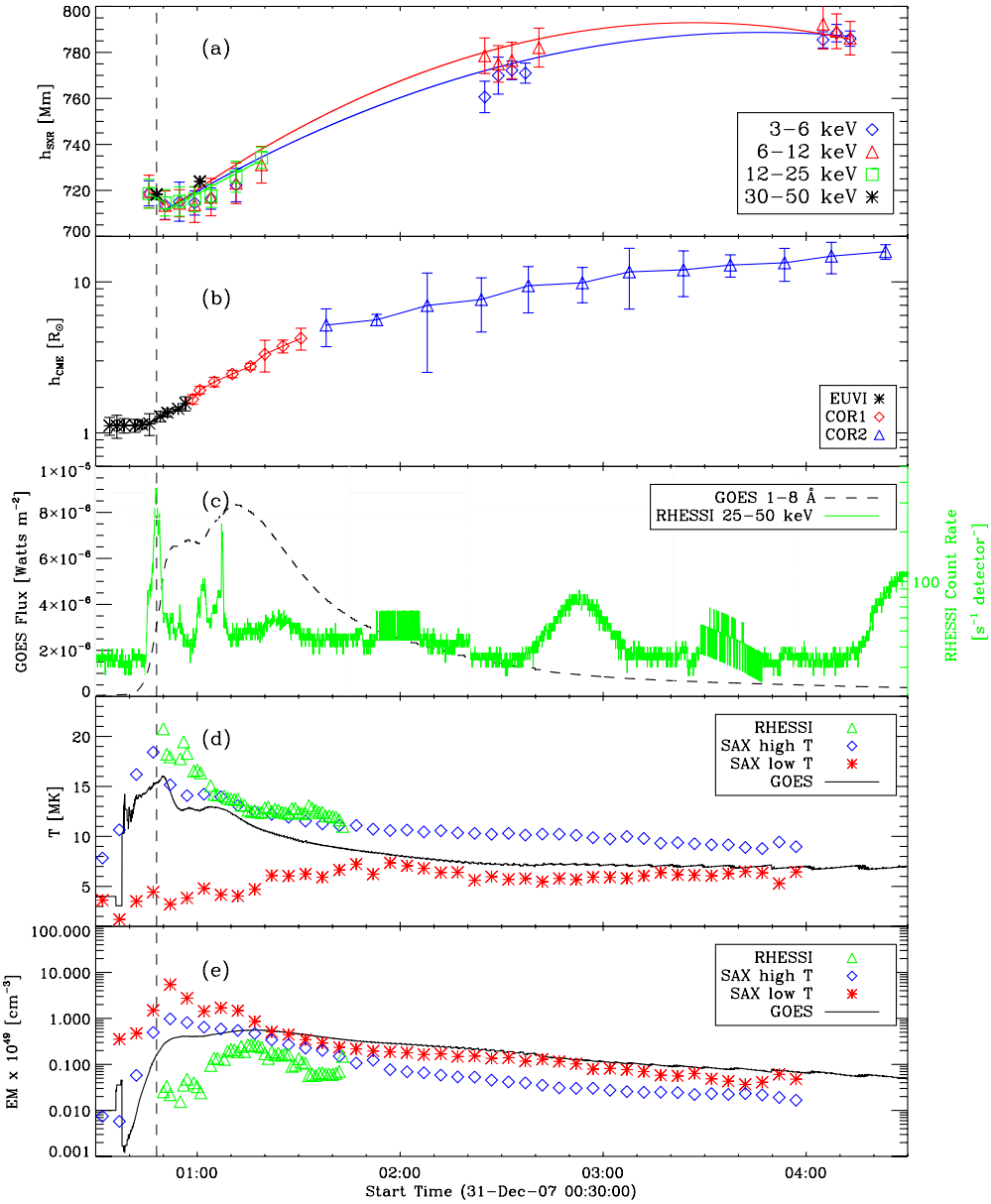

Figure 5. (a) SXR displacement from Sun center for 3–6 (blue diamonds), 6–12 (red triangles), 12–25 keV (green squares), and 30–50 keV (black asterisks) sources, fit with constant acceleration models. (b) CME apex displacement from Sun center for EUVI 171 Å (black asterisks), Cor 1 (red diamonds), and Cor 2 (blue triangles). (c) *GOES* 1–8 Å SXR light curve (black dashed line) and *RHESSI* 25–50 keV light curve (green solid line). (d) Flare temperature measured by *GOES* (black solid line), *RHESSI* (green triangles), SAX high- (blue diamonds), and low-temperature (red asterisks) components. (e) Flare emission measure from *GOES*, *RHESSI*, and SAX.

(A color version of this figure is available in the online journal.)

This is clearly observed during the 2007 December 31 event (Figures 4 and 5(a)). In addition, Sui & Holman (2003) hypothesize the formation of a current sheet between the thermal and non-thermal sources. Krucker et al. (2010) state that the 30–50 keV source observed during the 2007 December 31 event describes the site of particle acceleration. Therefore, should particles be accelerated at this non-thermal source and propagate down to heat the loop-top plasma, generating a thermal source, it may be the case that a current sheet forms between these two sources, as hypothesized by Sui & Holman (2003).

The timing in this event is crucial for the interpretation of the driving mechanism. This event began at ∼00:46 UT with the appearance of an SXR source at a height of 22 ± 1 Mm above the photosphere. This corresponds very closely to the height of the pre-eruption arcade loops. At this time, the temperature of the region had risen from its equilibrium value of 5 ± 2 MK to 19 ± 2 MK (see Figure 5(d)). The rise in temperature and the presence of an SXR source imply that magnetic reconnection had taken place before the CME is launched. This is characteristic of the slow magnetic reconnection events hypothesized by Moore & Roumeliotis (1992) for tether-cutting mechanisms. Moore & Roumeliotis (1992) suggested that the most likely cause of this slow, pre-eruption reconnection is flux cancelation either through the reconnection of an emerging flux system with the existing system, or photospheric motions reducing the distance between neighboring (or overlying) loop systems. As this particular event occurred on the limb, it is not possible to analyze magnetograms to determine the level of flux

emergence or cancelation. Regardless, the presence of X-ray sources before the launch of the CME immediately rules out the ideal MHD trigger as a mechanism for CME initiation. In addition, the position of the SXR and HXR sources beneath the CME before launch are not in good agreement with the breakout model, where particle acceleration is initially expected above the erupting CME and not beneath it. Therefore, the internal tether-cutting mechanism best fits our observations.

Having observed pre-eruption reconnection with SXR and HXR sources located at the top of the arcade loops (indicators of internal tether-cutting), a second period of HXR fluctuations between 00:57 UT and 01:10 UT was observed. During this period, the CME underwent a secondary burst of acceleration, described in detail in Lin et al. (2010). Imaging these late HXRs revealed an elongated source located between the post-flare arcade and the base of the CME (Figure 3(c), right panel). This HXR source was found to be co-spatial with the straight structure observed in the left panel of Figure 3(c). This may imply that the formation of a current sheet between the legs of the CME and above the post-flare arcade around this time facilitated continuous reconnection as the CME propagates away from the Sun. Thus, the evolution of this event is interpreted as follows.

1. The system was destabilized by slow, pre-eruption reconnection.
2. Internal tether-cutting magnetic reconnection along a current sheet formed between the legs of the arcade began to occur, untethering the plasmoid from the photosphere and generating a flare beneath the reconnection site.
3. As the CME erupted, X- to Y-type magnetic reconnection progressed along the top of the arcade, elongating the SXR source.
4. The rate of magnetic reconnection between the CME and post-flare arcade increased with the implied formation of the current sheet, thus increasing the HXR flux.
5. The CME propagated away and the post-flare arcade evolved.

The unique multi-spacecraft observations used for this study, specifically the high spectral resolution of SAX, enabled a detailed analysis of the hydrodynamic evolution of an eruptive flare. High-resolution data from the *STEREO* and *RHESSI* instruments allowed the kinematic evolution of both the flare and the CME to be analyzed simultaneously. We present a complete overview of the processes involved in the CME eruption and flare initiation. Our results clearly demonstrate that there is a physical connection between the flare and the CME. The approach taken here has allowed for the disregard of two out of three possible theoretical models and allowed the authors to establish that this event was most likely initiated by an internal tether-cutting process. We understand these to be the first clear observations of an event driven by the internal tether-cutting mechanism as it undergoes the transformation from X- to Y-type reconnection.

C.L.R. and C-H.L. are supported by an ESA/Prodex grant administered by Enterprise Ireland. R.T.J.McA is a Marie Curie Fellow, funded under EU FP6. We thank the anonymous referee for their helpful comments and for helping to improve the overall understanding of this paper.

REFERENCES

Antiochos, S. K. 1998, ApJ, 502, L181
Antiochos, S. K., DeVore, C. R., & Klimchuk, J. A. 1999, ApJ, 510, 485
Chen, P. F., & Shibata, K. 2000, ApJ, 545, 524
Forbes, T. G., & Isenberg, P. A. 1991, ApJ, 373, 294
Forbes, T. G., & Priest, E. R. 1995, ApJ, 446, 377
Gallagher, P. T., Dennis, B. R., Krucker, S., Schwartz, R. A., & Tolbert, A. K. 2002, Sol. Phys., 210, 341
Gallagher, P. T., Lawrence, G. R., & Dennis, B. R. 2003, ApJ, 588, L53
Gosling, J. T. 1993, J. Geophys. Res., 98, 18937
Harrison, R. A., & Bewsher, D. 2007, A&A, 461, 1155
Howard, R. A., et al. 2008, Space Sci. Rev., 136, 67
Hudson, H., Haisch, B., & Strong, K. T. 1995, J. Geophys. Res., 100, 3473
Isenberg, P. A., Forbes, T. G., & Demoulin, P. 1993, ApJ, 417, 368
Kaiser, M. L., Kucera, T. A., Davila, J. M., St. Cyr, O. C., Guhathakurta, M., & Christian, E. 2008, Space Sci. Rev., 136, 5
Krucker, S., Hudson, H. S., Glesener, L., White, S. M., Masuda, S., Wuelser, J.-P., & Lin, R. P. 2010, ApJ, 714, 1108
Lin, C. H, Gallagher, P. T., & Raftery, C. L. 2010, A&A, 516, A44
Lin, R. P., Dennis, B. R., & Benz, A. O. 2002, Sol. Phys., 210, 3
Moore, R. L., & Roumeliotis, G. 1992, in Proc. IAU Colloq. 133, Eruptive Solar Flares, ed. Z. Svestka, B. V. Jackson, & M. E. Machado (New York: Springer), 69
Moore, R. L., & Sterling, A. C. 2006, in Solar Eruptions and Energetic Particles, ed. N. Gopalswamy, R. Mewaldt, & J. Torsti (Geophysical Monograph Ser. 165; Washington, DC: American Geophysical Union), 43
Raftery, C. L., Gallagher, P. T., Milligan, R. O., & Klimchuk, J. A. 2009, A&A, 494, 1127
Reames, D. V. 1995, EOS Trans. Am. Geophys. Union, 76, 405
Roussev, I. I., Forbes, T. G., Gombosi, T. I., Sokolov, I. V., DeZeeuw, D. L., & Birn, J. 2003, ApJ, 588, L45
Santo, A. G., et al. 2001, Planet. Space Sci., 49, 1481
Schlemm, C. E., et al. 2007, Space Sci. Rev., 131, 393
Schwartz, R. A., Csillaghy, A., Tolbert, A. K., Hurford, G. J., Mc Tiernan, J., & Zarro, D. 2002, Sol. Phys., 210, 165
Sui, L., & Holman, G. D. 2003, ApJ, 596, L251
Švestka, Z. 2001, Space Sci. Rev., 95, 135
Temmer, M., Veronig, A. M., Vršnak, B., Rybák, J., Gömöry, P., Stoiser, S., & Maričić, D. 2008, ApJ, 673, L95
Thomas, R. J., Crannell, C. J., & Starr, R. 1985, Sol. Phys., 95, 323
Tripathi, D., Isobe, H., & Mason, H. E. 2006, A&A, 453, 1111
Zhang, J., Dere, K. P., Howard, R. A., Kundu, M. R., & White, S. M. 2001, ApJ, 559, 452